Diffractive hyperchromatic objective for chromatic confocal microscopy

JIABIN CHEN,[†] SHAOBAI LI,[†] WENJUN KANG,[†] (ID) SHUYUAN GUAN, ZHIHAN HONG, AND RONGGUANG LIANG[*] (ID)

Wyant College of Optical Sciences, The University of Arizona, Tucson, Arizona 85721, USA
[†]These authors contributed equally to this work.
[*]*rliang@optics.arizona.edu*

Abstract: The limited focal shift of conventional achromatic objectives constrains the maximum imaging depth of chromatic confocal microscopes. To address this, we designed a hyperchromatic confocal microscope using diffractive optical elements, which was fabricated by single-point diamond turning (SPDT). This design takes advantage of the small Abbe number of diffractive optical elements to introduce a significant longitudinal chromatic shift. The resulting chromatic confocal microscope achieved a maximum imaging depth of 750 μm and a lateral resolution of 0.78 μm across a wavelength range of 600–810 nm. The system's imaging capabilities were demonstrated by capturing detailed images of biological samples, including cucumber seed cavities, pig kidney, and human forearm skin. These results confirmed the microscope's effectiveness in visualizing key cellular structures, underscoring its potential for high-resolution biological imaging.

1. Introduction

The confocal microscope provides the ability to image deep into tissues with high-resolution, and optical sectioning, enabling 3D reconstructions of imaged samples [1–4]. Typically, volumetric imaging is achieved by piezo scanning along the Z-axis. However, this mechanical axial scanning is time-consuming and can introduce motion artifacts [5]. In recent years, chromatic confocal technology has gained attention for its ability to provide high-resolution imaging across multiple depths without the need for mechanical scanning.

Chromatic confocal microscopy employs the principle of chromatic dispersion, wherein broadband light passing through a lens is subject to wavelength-dependent variations in the refractive index, causing each wavelength to focus at distinct points along the optical axis. By utilizing a dispersion element, the optical axis can be encoded with wavelength-specific depth information [6–10]. Consequently, this enables multi-depth imaging without the mechanical limitations of traditional confocal microscopes, making it a valuable tool in both metrology and biological imaging, especially when a large scan range is required [11–14].

However, most of the commercial objectives are designed for achromatic applications with limited focal shifts, restricting the maximum imaging depth in chromatic confocal microscopes. Maitland et al. addressed this by adding two aspherical lenses in their system, achieving a focal shift of 160 μm [15]. In previous work, we employed a digital mirror device-based chromatic confocal microscope and achieved a 45 μm focal shift through 505-650 nm wavelength range [16]. Wang et.al developed a chromatic confocal endoscope with a customized objective [17]. They achieved an 800 μm focal shift from 650-950 nm, but the lateral resolution was limited by its numerical aperture (NA). They also presented a time stretch chromatic confocal microscope with 5 Hz volumetric imaging speed [18]. Fainman et.al demonstrated using a diffractive lens for non-mechanical depth scanning with a 55 μm shift [19]. Unlike traditional lenses, the diffractive lens offers material-independent dispersion. When the wavelength turning range is much less than the designed wavelength, the focal depth is linear to the wavelength and thus can be characterized

analytically. Despite these advances, there remains a need for chromatic objectives with both large focal shifts and high numerical apertures, especially for biomedical imaging, where cellular structures must be resolved.

Such an objective lens should possess significant longitudinal chromatic aberration to encode depth information over a broad spectral range while being well-corrected for monochromatic aberrations such as spherical aberration, coma, astigmatism, and field curvature. This ensures diffraction-limited performance at each wavelength within the operational bandwidth, especially for various biomedical imaging applications [20]. Additionally, the objective must offer a high numerical aperture (NA) to enhance resolution and light collection, as well as a field of view (FOV) that minimizes off-axis aberrations and allows for larger sample areas to be imaged without compromising quality. Consequently, we aim to develop a specially designed objective lens tailored to the specific requirements of our biomedical imaging applications combining a large longitudinal chromatic aberration for extended depth range measurements with corrections for monochromatic aberrations.

In this work, we present a diffractive optical element based objective lens with a 750 μm chromatic shift and a NA of 0.7, fabricated using a SPDT machine. This objective enables our chromatic confocal system to capture a wide range of depth information simultaneously without stage scanning, maintaining a lateral resolution of 0.78 μm. Biological tissues were visualized under this microscope to evaluate its performance.

2.　Method

2.1.　Objective design

Longitudinal chromatic aberration means the focus of the light varies with different wavelengths. The longitudinal focal shift can be written as:

$$\Delta s'_\lambda = -\frac{4F_{\#}^2}{n'}\partial_\lambda W_{020} \tag{1}$$

where n' and $F_{\#}$ are the refraction index and the working F-number in the imaging space and $\partial_\lambda W_{020}$ is the longitudinal chromatic wave aberration. When considering an optical system consisting of thin lenses, which are idealized models of lenses with negligible thickness but possessing optical power, certain calculations can be simplified as:

$$\partial_\lambda W_{020} = \frac{1}{2}\sum_{i=1}^{n}\left[\frac{\phi_i}{V_i}y^2\right] \tag{2}$$

Here, the ϕ_i is the optical power of ith element, y is the marginal ray height, and V_i is the Abbe number, which represents the dispersive behaviour of the optical elements.

To enhance chromatic aberrations, preferential use of low Abbe number glasses with significant refractive index differences across various wavelengths is recommended. The Abbe number v_{ref} for the refractive lenses is determined by the refractive index of the lens material at selected wavelengths as:

$$v_{ref} = \frac{n_d - 1}{n_F - n_C} \tag{3}$$

Here, the indices characterize specific wavelengths (λ_d=587.5618 nm, λ_F=486.1327 nm, and λ_C=656.2725 nm). However, with increasing wavelength, the diminishing disparity in refractive index results in reduced chromatic shift, particularly noticeable in the NIR range. In addition to refractive lenses, diffractive elements are also useable in hyperchromatism. The Abbe number of

diffractive elements is only dependent on the reference wavelengths as [21]:

$$v_{diff} = \frac{\lambda_d}{\lambda_F - \lambda_C} = -3.4534 \tag{4}$$

The small absolute value of the diffractive Abbe number implies a substantial dispersion effect.

In Zemax, the diffractive surface bends rays according to the grating equation. The Binary 2 surface allows the grating period to vary as a rotationally symmetric polynomial. It uses the phase advance or delay to alter the direction of ray propagation. The Binary 2 surface adds phase to the ray according to the following equation no matter what the wavelength is:

$$\phi(\rho) = m \sum_{i=1}^{n} A_i \rho^{2i} \tag{5}$$

where $\phi(\rho)$ is the phase in periods at radius ρ, n is the number of the polynomial coefficients in the series, A_i is the coefficient on the 2^i power of ρ, which is the normalized radial coordinate, m is the diffraction order. The coefficient A_1 of Eq. (4) is the determinant of the diffractive surface optical power when m = 1:

$$\varphi(\lambda) = \frac{1}{f} = \lambda A_1 \tag{6}$$

It means that different wavelengths will give different optical powers.

It is worth noting that the chromatic shift is also proportional to the square of the $F_\#$ based on Eq. (1). This relationship implies that achieving significant hyperchromatization becomes increasingly challenging for fast optical systems with high numerical apertures (low $F_\#$). Consequently, for such high-performance applications requiring high NA, a more complex hybrid diffractive-refractive optical design is often necessary. The synergistic combination of diffractive and refractive components in a hybrid optical design allows for greater flexibility in manipulating the chromatic behavior and aberration control of the system, enabling the simultaneous achievement of high numerical apertures and significant chromatic shifts. By optimizing the focal power distribution between the diffractive and refractive components, and optimizing the lens shape and diffractive surfaces, a high-performance hyperchromatic objective can be realized [20–22]. Additionally, the total longitudinal chromatic aberration is also influenced by the sign of the optical power based on Eq. (1). Specifically, when the optical power of the diffractive element is negative, neglecting the effect of radius, this can lead to a situation where the shorter wavelength results in a shorter focal length. The hyperchromatic objective lenses were designed and optimized in Zemax using multiconfiguration. Related merit functions were established to control longitudinal chromatic aberration and image quality between wavelengths. Meanwhile, the NA, focal length of the lens and other intrinsic restrictions were locked to reach the specification. During the optimization process, the diffractive surface terms were managed to ensure that the diffractive zones were not too densely packed, allowing for manufacturability using diamond turning technology. In this design, the coefficients of p^2 and p^4 are set to variables for optimization. The merit function should ensure telecentricity in the image space, which is vital for maintaining consistent image quality across different focal planes. We also accounted for the marginal ray height, as it strongly influences longitudinal chromatic aberration. As a result, a large-scale diffractive element could further increase the focal shift, which is key to controlling the chromatic performance of the system.

The layout of our objective is detailed in Fig. 1(A-C). The bandwidth of the source is selected from 600 nm to 810 nm to reduce scattering from the tissue. The corresponding chromatic shift is about 750 µm. The designed hyperchromatic objective achieves a NA of 0.7 in water across ±0.4 mm lateral field. It offers 40x magnification through a 200 mm focal length tube lens. Table 1 summarizes the capabilities of the system.
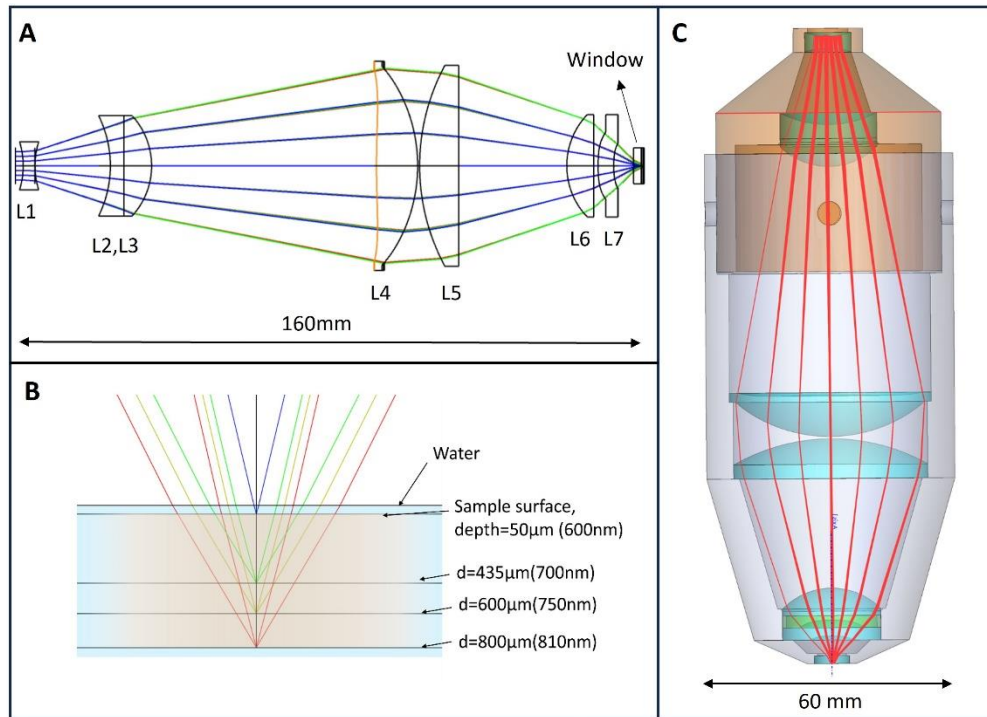
Fig. 1. (A) Optical layout of the designed objective. (B) Magnified view showing chromatic shift along the tissue depth. (C) Final objective lens with mechanical housing.

Table 1. Specification of the chromatic objective

Specification	Value
NA	0.7
Focal length	5mm
Field of view	±0.4mm
Wavelength range	600-810nm
Chromatic shift	~750um
Working distance	50-800um
Material (DOE)	PMMA
Outer Diameter	60mm
Off-the-shelf lens	L1, L2, L3, L5, L6

To streamline the manufacturing process, we decided to combine off-the-shelf lenses with two custom diamond-turned lenses to realize the final design. Figure 1 shows the layout of the hyperchromatic objective lens, which has a total length of 160 mm and an outer diameter of 60 mm. It was composed of 5 off-the-shelf lenses (L1, L2, L3, L5, L6) and two diamond-tuned PMMA lenses (L4, L7) as shown in Fig. 1(A). L4, which acts as the system stop, features a front-surface even aspheric design and a rear diffractive surface, correcting spherical aberrations and enhancing chromatic shift. L7 is also an aspheric lens used to correct off-axis aberrations. The final optical performance of the objective lens was evaluated by controlling the spot size on the image plane. Figure 2(A-D) show the Modulation Transfer Function (MTF), chromatic shift among 600-810 nm, RMS wavefront, and spot diagram errors across the field of view (FOV) at

700 nm, confirming that the lens performs at the diffraction limit. Additional wavelengths can be found in Fig. S1.
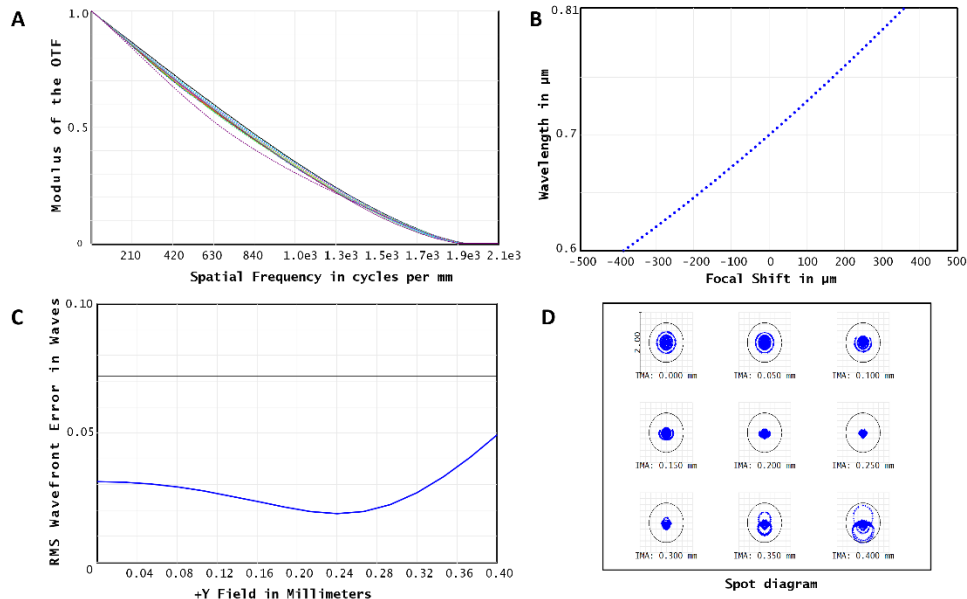
Fig. 2. Performance of the designed objective lens at 700 nm. (A) MTF. (B) Chromatic shift. (C) RMS wavefront error. (D) Spot diagram.
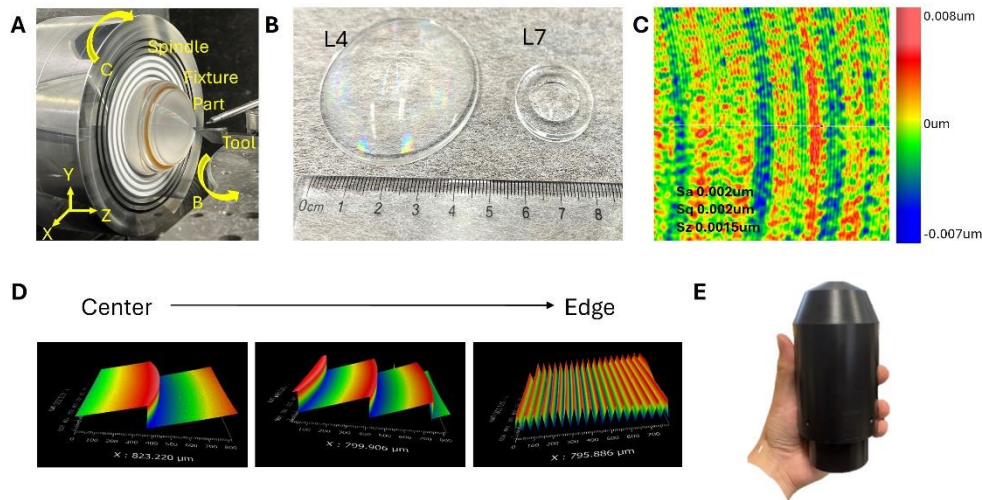
2.2. Fabrication

The diffractive lens and aspheric lens are both fabricated by SPDT (Moore Nanotech 350FG). SPDT is a subtractive manufacturing process that utilizes a contour-controlled diamond tool slide across materials like ductile metal, plastics, and infra-red glasses etc., the motion is coordinated by a precision computer numerically controlled machine [23,24]. It is typically used to rapidly prototype high-precision optical elements and systems, including both axial symmetrical and freeform ones [24,25]. This technique typically achieves nanometer-level surface roughness and sub-micrometer-level surface form accuracy.

In our experiment, both diffractive lens L4 and aspheric lens L7 were customized SPDT fabricated and evaluated. They were made of PMMA with Moore Nanotech 350FG, and the machining configuration is shown in Fig. 3(A). To ensure the fine diffractive structure's fabrication, a concurrent engineering method was deployed, with manufacturing limitations considered during the initial design phase. Here, in the machining phase, a small half-radius diamond tool was used with small stepping and efficient chip removal techniques. As a result, the finished lenses are shown in Fig. 3(B) correspondingly. To ensure their performance, surface measurements have been carried out with Zygo Newview 8300 white light interferometer, achieving less than 10 nm surface roughness, as shown in Fig. 3(C). Additionally, micro-structures on the diffractive surface were also measured and verified. As shown in Fig. 3(D), the diffractive periods become denser from the center to the edge while maintaining consistent height, closely matching the design specifications.

Besides the optical components, a housing system was designed and fabricated to securely mount and position the lenses, as shown in Fig. 3(E). A common fiducial datum was established and utilized for precise alignment. The housing is divided into two main body sections located at the air gap between L3 and L4, where sensitivity to tolerances is minimal according to sensitivity

Fig. 3. Fabricated objective lens and measurement result. (A) SPDT configuration. (B) Diamond turned diffractive lens and aspheric lens. (C) Surface profile under the white light interferometer. The surface roughness is less than 10 nm over the whole area. (D) Diffractive surfaces from center to edge. (E) Custom holders for objective lens assembly.

analysis. Furthermore, the axial distance between these two body sections can be adjusted, allowing for active alignment of the objective lens, which also serves as a focus compensator.

3.   Result

We developed a chromatic confocal microscope with the designed hyperchromatic objective as shown in Fig. 4(A). The broadband source (NKT SuperK Extreme) was filtered to generate light from 600 to 810 nm. Two lenses were used to magnify the beam size to fulfill the entrance pupil of the objective. The scanning in the XY direction was conducted by the 2D Galvo scanner (Thorlabs GVS212). And two relay lenses ensure the beam is telecentric at the pupil. Then, after passing through the objective, the different wavelengths focus at different depths. The reflected light containing depth information passed through a pinhole and was then spectrally separated by a grating (Ibsen FSTG-VIS1379-911, grating resolution 1379 l/mm). A USB line detector (Coptonix S11639-01, 2048pixels) is used to detect spectrum information enabling simultaneous depth information acquisition. A LabVIEW-based software was written to control synchronization and data acquisition. The synchronization between the Galvo scanners and the line detector was achieved using a PCIe-6361 data acquisition board (National Instruments). The acquisition board generated a continuous digital pulse signal that triggered both the Galvo scanners and the line detector in synchronization. This ensured that each line scan from the detector corresponds precisely with the correct spatial position from the Galvo system. The duty cycle of this pulse signal was determined by the integration time of the line camera, meaning that the exposure time directly controls the timing of each step in the Galvo scan. A Boolean control signal manages the initiation of the scan and the start of data acquisition to ensure they are perfectly aligned. For each 3D volume scan, we captured $512 \times 512 \times 2048$ pixels, where 512×512 represented the lateral resolution across each en face image, and 2048 pixels corresponded to the axial depth sampling. The saved images were resliced to present the en face information. The volumetric acquisition took approximately 5 minutes in the tissue imaging. The imaging speed of chromatic confocal microscopes is influenced by several factors, including laser

power, detector sensitivity, read out speed, and the reflectance of the sample [26]. The current speed was mainly limited by the sensitivity and line read out time of the USB line detector.
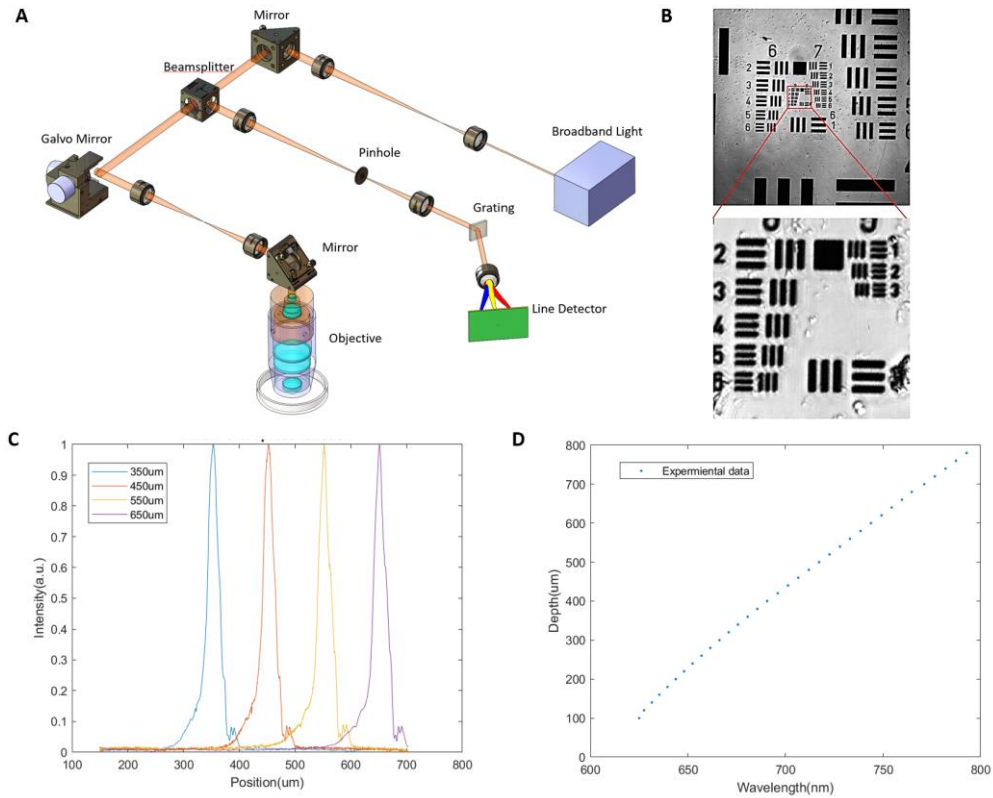

Fig. 4. (A) Setup of the chromatic confocal microscope. (B) Measurement of lateral resolution. Group9 Element 3 is visualized. (C) The axial point spread function shows the axial resolution is about 20 µm. (D) Experiment data results between focus depth and wavelength.

A standard 1951 USAF resolution target was placed to measure the lateral resolution. Group 9, Element 3 was visualized, as shown in Fig. 4(B), indicating a lateral resolution of 0.78um. The axial point spread function shown in Fig. 4(C) is measured through a movable flat mirror, and the axial resolution is about 20 µm. Figure 4(D) shows the experimental result of the system between the focus depth and wavelength. The maximum imaging depth is about 750 µm. These results confirm the system's capability for high-resolution, depth-resolved imaging across a substantial depth range, highlighting its potential for diverse applications in optical microscopy.

To demonstrate the imaging capabilities of chromatic confocal microscope, we conducted imaging of the folded lens tissue paper, multilayer tape, onion, and cucumber. Figure 5 shows the depth color-coded, en face, cross-sectional and 3D images of these samples. Different colors represent different depths. The thickness of each tape layer is 50 µm. The maximum imaging depth in the cucumber seed cavity is about 250 µm. These results confirm the 3D imaging performance of the system.

To further explore the feasibility of this chromatic confocal microscope in biological imaging. We also captured images from turbid tissue samples, and Fig. 6(A) shows the depth color-coded, en face, cross sectional images of the thick pig kidney tissue. Figure 6(B) displays images at various depths (40–140 µm), revealing the tubule structures. Then, we obtained some en face
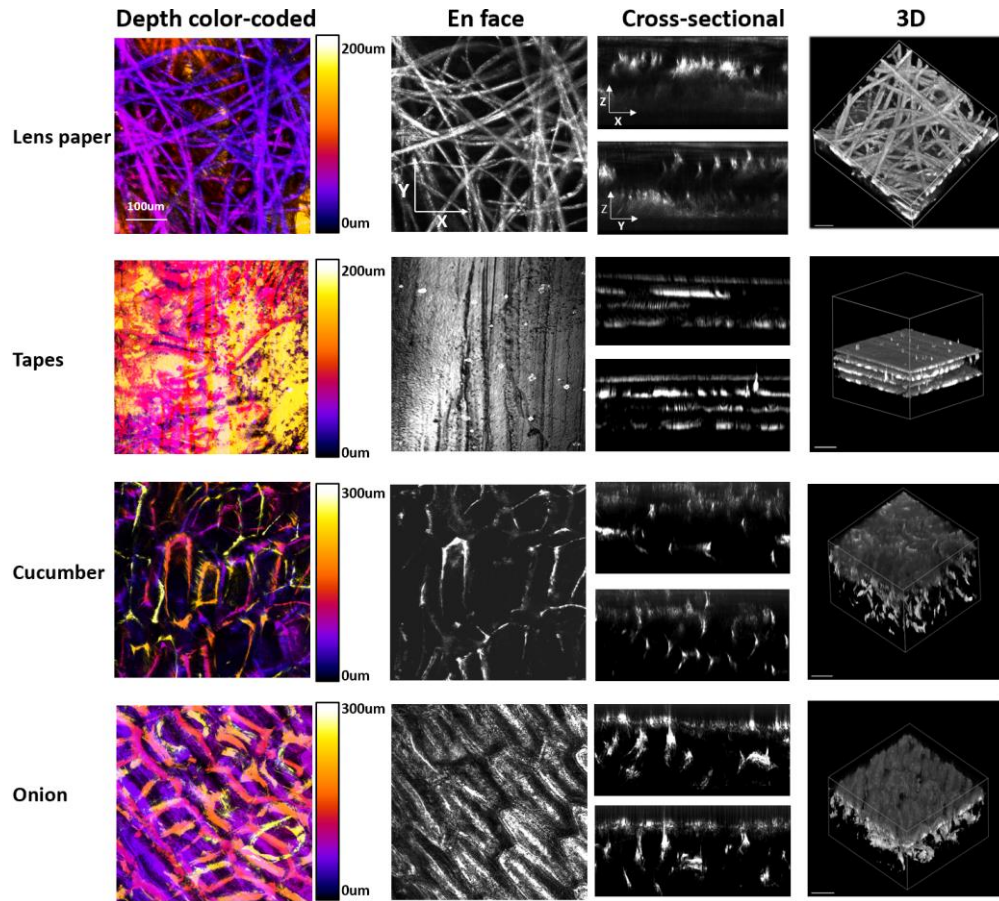
Fig. 5. Imaging performance of the system. Depth color-coded, en face, cross-sectional and 3D images collected from the folded lens tissue paper, multilayer tapes, cucumber seed cavity and onion. Scale bar 100 μm.

images from the human forearm skin, as shown in Fig. 7. The dermal papillae are surrounded by brightly pigmented keratinocytes and melanocytes. These results collectively highlight the potential of chromatic confocal microscopy as a versatile tool for high-resolution imaging across various types of samples, including both inanimate and biological tissues.

Biomedical Optics EXPRESS
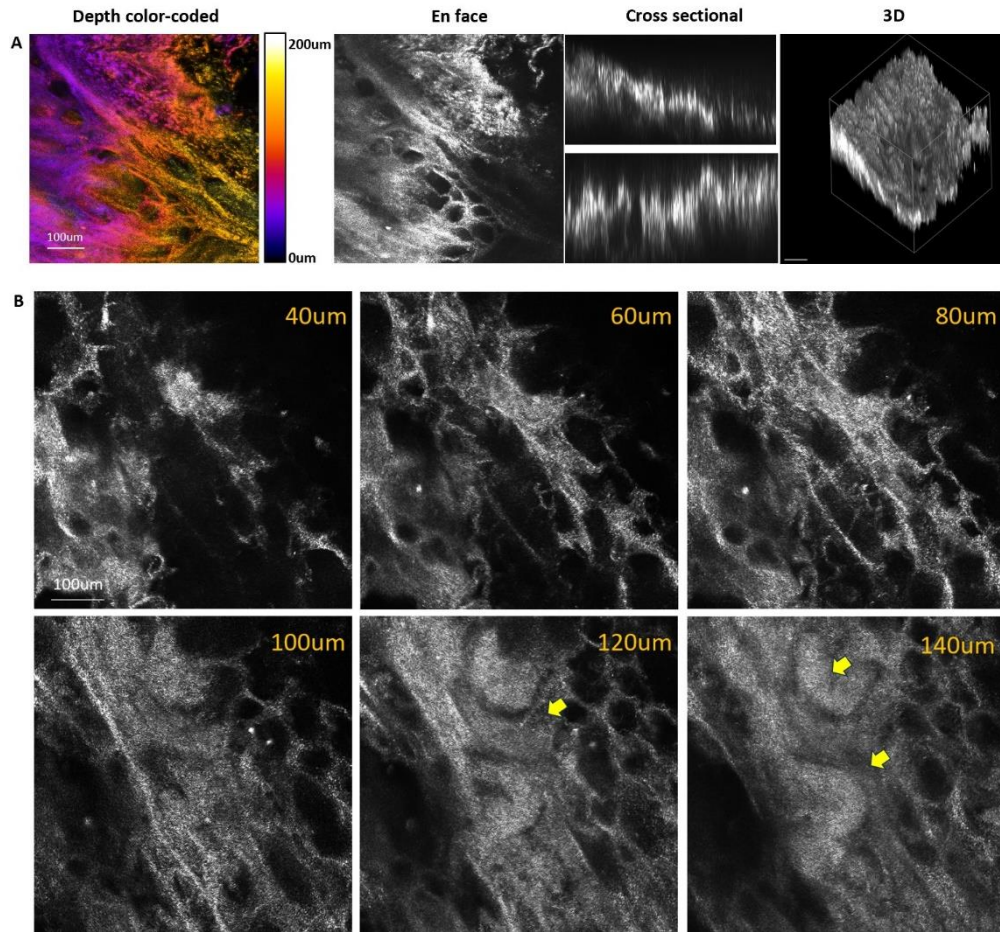
Fig. 6. (A)Depth color-coded, en face and cross-sectional images of the pig kidney. Different colors represent different depths. (B) Kidney images at different depths. Tubule structures are visualized (yellow arrow).
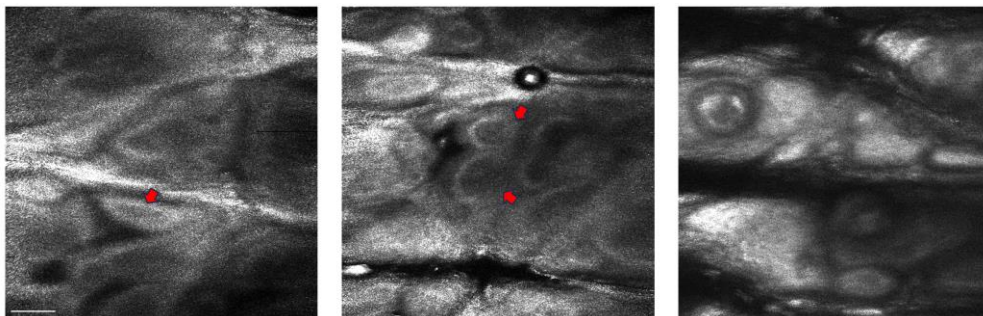
Fig. 7. Images of human forearm skin at different locations. The dermal papillae are surrounded by brightly pigmented keratinocytes and melanocytes (red arrow). Scale bar 100um.

4.   Discussion

In this study, we have designed and fabricated a diffractive hyperchromatic objective characterized by a chromatic focal shift of 750 μm and a NA of 0.7. This objective was engineered to optimize monochromatic aberrations across a spectral range from 600 to 810 nm. The design parameters and aberration corrections make our objective particularly suitable for use in a chromatic confocal microscope, facilitating both subcellular resolution and significant imaging depth.

The manufacturing of the microscope objective involved the use of SPDT to achieve precise control over the surface shape. The surface quality of the objective was rigorously evaluated using a white light interferometer, resulting in a surface roughness of less than 10 nm. This level of surface precision is critical for maintaining optical performance and achieving high-resolution imaging.

The corresponding chromatic confocal microscope system, equipped with the hyperchromatic objective, demonstrated a lateral resolution of 0.78 μm and a maximum imaging depth of 750 μm. These performance metrics highlight the system's capability to deliver detailed and deep imaging.

To validate the imaging capabilities of our chromatic confocal microscope, we conducted imaging experiments on various biological tissues, including kidney and skin samples. The imaging results illustrated that the microscope could effectively visualize key subcellular structures, thereby underscoring its potential for high-resolution biological imaging applications. These findings demonstrate the effectiveness of our optical system in achieving both the necessary resolution and depth for advanced microscopy tasks. However, the 3D acquisition time for tissue imaging was limited to approximately 5 minutes due to the sensitivity and line readout speed of the USB detector. In the future, we will explore suitable high-speed line detectors to increase imaging speed. Improved imaging performance can be achieved with higher speeds and an adequate number of average frames.

There are still some downsides to this objective lens. The fabricated lens housing fails to provide sufficiently precise air gap control, compromising the desired accuracy. The shoulder on the axial point spread function shows the residual aberration and may reduce the image contrast. Concurrently, the peripheral surface profiles of the commercially available off-the-shelf lenses are inadequate for high NA imaging applications. To further introduce large longitudinal chromatic aberration, we increased the marginal ray height which sacrifices the overall form factor. The microscope design features a high magnification of 40x, which poses a challenge in initially locating the region of interest or identifying the imaging target within the relatively confined FOV. The narrow FOV resulting from the substantial magnification can hinder the initial search and acquisition of the desired sample area or object. Addressing these issues will require further design optimization and improvements in the fabrication process. Future work will focus on reducing the form factor of the lens assembly and ensuring precise mounting for each lens element. These enhancements are expected to mitigate the current limitations and significantly improve the imaging performance of the objective lens.

Disclosures. The authors declare that they have no conflict of interest.

Data availability. Data underlying the results presented in this paper are not publicly available at this time but may be obtained from the authors upon reasonable request.

Supplemental document. See Supplement 1 for supporting content.

Reference

1. G. S. Kino and T. R. Corle, *Confocal Scanning Optical Microscopy and Related Imaging Systems* (Academic Press, 1996).
2. A. Levine and O. Markowitz, "Introduction to reflectance confocal microscopy and its use in clinical practice," JAAD Case Reports **4**(10), 1014–1023 (2018).

3. J. Pawley, "Handbook of biological confocal microscopy," Springer google schola **2**, 1035–1040 (2006).
4. H. J. Tiziani, R. Achi, R. N. Kramer, *et al.*, "Chromatic confocal microscopy with microlenses," J. Mod. Opt. **43**(1), 155–163 (1996).
5. J. T. Fredrich, "3D imaging of porous media using laser scanning confocal microscopy with application to microscale transport processes," Physics and Chemistry of the Earth, Part A: Solid Earth and Geodesy **24**(7), 551–561 (1999).
6. H. J. Tiziani and H.-M. Uhde, "Three-dimensional image sensing by chromatic confocal microscopy," Appl. Opt. **33**(10), 1838–1843 (1994).
7. Z. Hong, Y. Sun, P. Ye, *et al.*, "Bio-Inspired Compact, High-Resolution Snapshot Hyperspectral Imaging System with 3D Printed Glass Lightguide Array," Adv. Opt. Mater. **11**(9), 2300156 (2023).
8. Z. Hong, P. Ye, D. A. Loy, *et al.*, "High-precision printing of complex glass imaging optics with precondensed liquid silica resin," Adv. Sci. **9**(18), 2105595 (2022).
9. Z. Hong, P. Ye, D. A. Loy, *et al.*, "Three-dimensional printing of glass micro-optics," Optica **8**(6), 904–910 (2021).
10. P. Ye, Z. Hong, D. A. Loy, *et al.*, "Solvent-Free Silsesquioxane Self-Welding for 3D Printing Multi-Refractive Index Glass Objects," Adv. Opt. Mater. **12**(23), 2400783 (2024).
11. F. Blateyron, "Chromatic Confocal Microscopy," in *Optical Measurement of Surface Topography*, R. Leach, ed. (Springer Berlin Heidelberg, 2011), pp. 71–106.
12. K. Shi, P. Li, S. Yin, *et al.*, "Chromatic confocal microscopy using supercontinuum light," Opt. Express **12**(10), 2096–2101 (2004).
13. J. Garzón, T. Gharbi, J. Meneses, *et al.*, "Real time determination of the optical thickness and topography of tissues by chromatic confocal microscopy," J. Opt. A: Pure Appl. Opt. **10**(10), 104028 (2008).
14. G. Sharma and K. Singh, "Ultralong imaging range chromatic confocal microscopy," Advanced Photonics Research **4**(1), 2200116 (2023).
15. C. Olsovsky, R. Shelton, O. Carrasco-Zevallos, *et al.*, "Chromatic confocal microscopy for multi-depth imaging of epithelial tissue," Biomed. Opt. Express **4**(5), 732–740 (2013).
16. S. Li and R. Liang, "DMD-based three-dimensional chromatic confocal microscopy," Appl. Opt. **59**(14), 4349–4356 (2020).
17. X. Yang, Y. Wang, H. Zhang, *et al.*, "Fiber-optic large-depth 3D chromatic confocal endomicroscopy," Biomed. Opt. Express **13**(1), 300–313 (2022).
18. X. Yang, H. Zhang, Z. Liu, *et al.*, "Time-stretch chromatic confocal microscopy for multi-depth imaging," Laser Photonics Rev. **17**(12), 2300387 (2023).
19. S. L. Dobson, P.-C. Sun, Y. Fainman, *et al.*, "Diffractive lenses for chromatic confocal imaging," Appl. Opt. **36**(20), 4744–4748 (1997).
20. J. Sasián, *Introduction to Lens Design* (Cambridge University Press, 2019).
21. M. Hillenbrand, B. Mitschunas, C. Wenzel, *et al.*, "Hybrid hyperchromats for chromatic confocal sensor systems," Adv. Opt. Technol. **1**(3), 187–194 (2012).
22. J. Garzón, "Diffractive elements performance in chromatic confocal microscopy," J. Phys.: Conf. Ser. **274**, 012069 (2011).
23. F. Fang, X.D. Zhang, A. Weckenmann, *et al.*, "Manufacturing and measurement of freeform optics," CIRP Ann. **62**(2), 823–846 (2013).
24. N. Khatri, K. Manjunath, S. Berwal, *et al.*, "Ultra-precision machining of optics," (2024).
25. W. Kang, M. Seigo, H. Xiao, *et al.*, "Experimental studies on fabricating lenslet array with slow tool servo," Micromachines **13**(10), 1564 (2022).
26. C.-S. Kim and H. Yoo, "Three-dimensional confocal reflectance microscopy for surface metrology," Meas. Sci. Technol. **32**(10), 102002 (2021).